Chapter 9
Reductive Conversion of Carbon Dioxide Using Various Photocatalyst Materials

Kojirou Fuku, Kohsuke Mori, and Hiromi Yamashita

9.1 Introduction

Although advances in science and technology have contributed to the development of society and have made people's lives increasingly comfortable, various environmental problems associated with technological advances have become global issues. In particular, global warming by greenhouse effect gas such as carbon dioxide (CO_2) and exhaustion of fossil fuels are already grave social problems of global dimensions. The catalytic conversion of CO_2 has widely been examined as one of the valuable approaches to solve these problems, but most of the processes require high temperature and pressures. However, various photocatalytic reactions have recently attracted considerable attention due to their milder reaction conditions (at room temperature and atmospheric pressure) and their ability to utilize solar light as inexhaustible energy source. Highly efficient and selective photocatalytic systems driven under sunlight and accompanied with a large positive change in the Gibbs free energy is of vital interest [1–8]. These reactions are considered to be an uphill reaction and are similar to the photosynthesis by green plants which produces glucose and oxygen from CO_2. The photocatalytic conversion of CO_2 emitted in large amounts into industrially beneficial compounds would be an alternative protocol from the viewpoints of *green and sustainable chemistry* by the solution of exhaustion of energy resources and global warming. Therefore, the development of efficient

K. Fuku
Division of Materials and Manufacturing Science, Graduate School of Engineering, Osaka University, 2-1 Yamada-oka, Suita, Osaka 565-0871, Japan

K. Mori • H. Yamashita (✉)
Division of Materials and Manufacturing Science, Graduate School of Engineering, Osaka University, 2-1 Yamada-oka, Suita, Osaka 565-0871, Japan

Elements Strategy Initiative for Catalysts Batteries ESICB, Kyoto University, Katsura, Kyoto 615-8520, Japan
e-mail: yamashita@mat.eng.osaka-u.ac.jp

B.M. Bhanage and M. Arai (eds.), *Transformation and Utilization of Carbon Dioxide*, Green Chemistry and Sustainable Technology, DOI 10.1007/978-3-642-44988-8_9,

photocatalytic systems enabling reduction and/or fixation of CO_2 is the most desirable and challenging goal [2, 3].

The utilization of solar energy for the conversion of CO_2 can be realized by considering the photocatalytic reduction and/or fixation of CO_2 into CO, HCOOH, CH_3OH, and CH_4, etc., by the active photocatalysts such as TiO_2, $SrTiO_3$, ZnO, or SiC semiconductors. Inoue and Fujishima et al. have first reported that HCOOH, HCHO, and CH_3OH are produced under irradiation of aqueous suspension systems involving a variety of semiconductor powders or single crystals [9]. Although the pioneering works on the photoreduction of CO_2 on semiconductors in aqueous suspension systems were summarized by Halmann, the efficiency was low when H_2O was used as the reductant [10]. Substantially improved yields of CH_3OH and CH_4 from CO_2 with H_2O have been reported by us, in which photocatalytic reactions successfully proceed in solid–gas systems at room temperature on isolated tetrahedral Ti centers of macro- or mesoporous silicate sieves instead of dense phase powdered TiO_2 materials [2, 3, 11–22]. We focus on the characteristic features of photocatalytic reduction and/or fixation of CO_2 with H_2O on various types of active titanium oxide catalysts under heterogeneous gas–solid conditions.

This review report about our approach on the efficient reduction and/or fixation of CO_2 using various titanium oxide photocatalysts. Additionally, other novel and unique systems enabling efficient conversion of CO_2 using various oxide semiconductors other than titanium oxide or localized surface plasmon resonance-enhanced photocatalysis are also introduced.

9.2 Various Titanium Oxide Photocatalysts

As shown in Fig. 9.1, the electronic properties as well as the photocatalytic activity of titanium oxide photocatalysts dramatically change depending on their local structure, from an extended semiconducting structure to nano-sized, extremely small nanoparticles and molecular-sized titanium oxide species. In the case of the bulk TiO_2 materials, photochemical excitation leads to charge separation in the particle, in which electrons (e^-) are promoted to the conduction band (cb) and holes (h^+) are left in the valence band (vb) upon light irradiation. The generated hole in the valence band and the conduction band electron can react with electron donors and electron acceptors adsorbed on the titanium oxide surface, respectively. On the contrary, the Ti-oxide moieties, which are spatially separated from each other, can be implanted and isolated in the silica matrixes of microporous zeolite and mesoporous silica materials at the atomic level, and have been named as “single-site photocatalysts.” The isolated Ti atoms can be substituted with Si atoms in the silica matrixes ($Si/Ti > 30$) and coordinated tetrahedrally with oxygen atoms. Such single-site catalysts can be simply synthesized by various anchoring techniques, such as hydrothermal synthesis, sol–gel method, and chemical vapor deposition, and are stable as far as the silica matrixes keep their porous structures. In the case of the isolated and tetrahedrally coordinated Ti-oxide moiety, excitation by UV irradiation brings about an electron transfer from the oxygen (O^{2-}) to Ti^{4+} ions, resulting in the

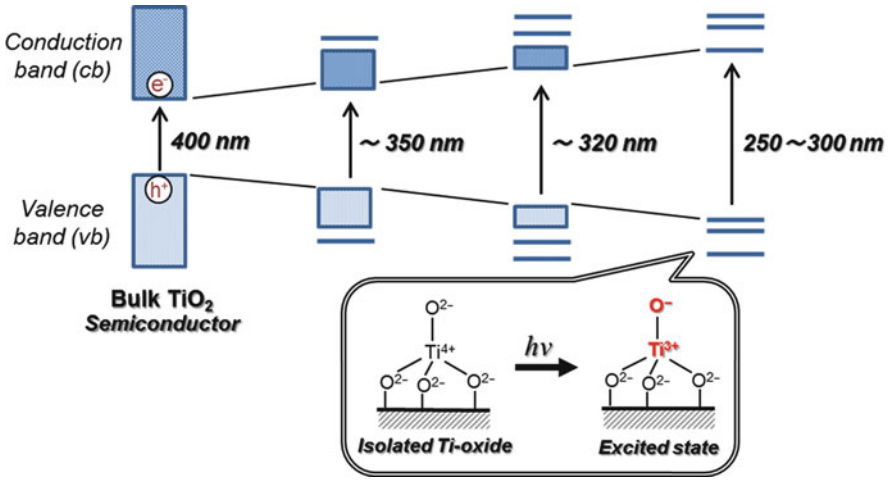

Fig. 9.1 The electronic state change in the titanium oxide photocatalysts from semiconducting bulk TiO_2 to the isolated Ti-oxide molecular species

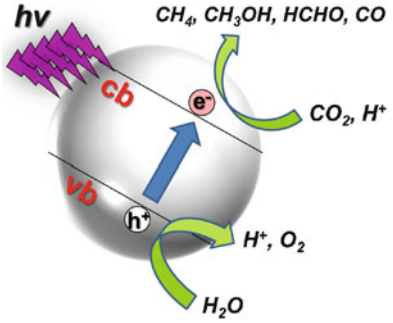

Fig. 9.2 Reaction scheme for the photocatalytic reduction of CO_2 with H_2O on bulk TiO_2

formation of pairs of trapped hole centers (O^-) and electron centers (Ti^{3+}). Such charge-transfer excited state, i.e., the excited electron–hole pair state which localizes quite near to each other as compared to the electron and hole produced in semiconducting materials, plays a significant role in various photocatalytic reactions.

The efficiency for the photocatalytic reduction and/or fixation of CO_2 with H_2O to produce CH_4 and CH_3OH strongly depends upon the type of the employed titanium oxide photocatalysts [11–22]. The primary processes on semiconducting TiO_2 photocatalysts are illustrated in Fig. 9.2. The band gap between the conduction band and the valence band becomes larger as the particle size of the semiconducting TiO_2 decreased, making it suitable and applicable to the reduction of CO_2 [2, 3]. For extremely fine TiO_2 particles less than 10 nm in diameter, the size quantum effect and/or the effects of the surface modification in its coordination geometry plays a significant role in the appearance of unique activity. Consequently, the electrons and holes which are produced by UV-light irradiation within the ultrafine particles of TiO_2 and the highly dispersed titanium oxide species exhibit more unique and high activities compared to those produced in large particle TiO_2 photocatalysts.

9.3 Small Particle TiO_2 Photocatalysts

UV irradiation of the powdered TiO_2 catalysts in the presence of a gaseous mixture of CO_2 and H_2O led to the evolution of CH_4 at 275 K, accompanied with the formation of trace amounts of C_2H_4 and C_2H_6 [13, 14]. The yields of these products increased with the UV-irradiation time, while no products were detected under dark conditions. The CH_4 yield was almost zero in the reaction of CO_2 without H_2O and increased with increasing the amount of H_2O. These results suggest that the photocatalytic reduction of CO_2 to produce CH_4 and C_2 compounds takes place photocatalytically in the solid–gas phase systems. The formation of CH_4 as the main product has also been observed by Saladin et al., and the partially reduced TiO_2 species formed under UV irradiation is proposed as an active species [23].

The yields of CH_4 formation in the photocatalytic reduction of CO_2 with H_2O on several TiO_2 photocatalysts with different physicochemical property are shown in Table 9.1. The photocatalytic activity, based on the CH_4 yields, was found to depend on the type of TiO_2 catalyst, in the order of JRC-TIO-4 > -5 > -2 > -3 [14]. This tendency corresponds with that in the photocatalytic hydrogenation of methyl acetylene with H_2O, proving that the reduction of CO_2 with H_2O undoubtedly occurs photocatalytically activated powdered TiO_2 catalyst [24, 25]. It is likely that the anatase-type TiO_2 possessing a large band gap as well as numerous surface –OH groups is preferable for efficient photocatalytic reactions. The band gap increase is accompanied by a shift in the conduction band edge to higher energy levels. This shift causes the reductive potential to shift to more negative values, which ultimately causes a great enhancement in the photocatalytic activity. The surface –OH groups and/or physisorbed H_2O also play a significant role in photocatalytic reactions via the formation of OH radicals and H radicals.

Preliminary studies by ESR measurement provide an insight into the reaction pathway. The ESR signals obtained under UV irradiation of the anatase-type TiO_2 catalyst in the presence of CO_2 and H_2O at 77 K can be ascribed to the characteristic photogenerated Ti^{3+} ions ($g_\perp = 1.9723$ and $g_\parallel = 1.9628$) and H radicals (with 490 G splitting), as well as CH_3 radicals having a hyperfine splitting ($H\alpha = 19.2$ G, $g = 2.002$) [14]. The signal intensity of CH_3 radicals decreased with increasing the amount of H_2O, indicating that CH_3 radicals are the intermediate species and react with H radicals that are formed by the reduction of protons (H^+) originated from H_2O adsorbed on the catalyst.

Table 9.1 Textural property and photocatalytic activity of TiO_2 catalysts

Catalyst	Crystal structure[a]	S_{BET} (m^2/g)	CO_2 ads. (μmol/g)	Relative –OH conc.	Band gap (eV)	Reduction of CO_2[b] (μmol/h·g)	Hydrogenation of methyl acetylene (μmol/h·g)
JRC-TIO-2	A	16	1	1	3.47	0.03	0.20
JRC-TIO-3	R	51	17	1.6	3.32	0.02	0.12
JRC-TIO-4	A	49	10	3.0	3.50	0.27	8.33
JRC-TIO-5	R	3	0.4	3.1	3.09	0.04	0.45

[a]A, anatase; R, rutile

[b]CH_4 yield in the reaction of CO_2 (0.12 mmol) and H_2O (0.37 mmol) for 6 h

9.4 Metal-Loaded TiO_2 Photocatalysts

The effect of metal loading on the photocatalytic reduction of CO_2 with H_2O on TiO_2 catalysts was investigated [14]. In the case of the Cu/TiO_2 photocatalyst (0.3–1.0 wt%), CH_4 yield was suppressed, but a new formation of CH_3OH could be observed. Characterization by XPS reveals that the main species of copper in the catalyst is 1+ oxidation state. It has been also reported that Cu^+ catalysts play a significant role in the photoelectrochemical production of CH_3OH from CO_2 and H_2O system [26]. Following the photocatalytic reduction, the Cu/TiO_2 catalysts exhibited a new peak at 299 eV in the C(1) XPS spectra, suggesting that carboxylate groups which accumulated on the catalyst may be the primary intermediate species for this reaction.

Further detailed study was performed by Gunlazuardi et al. by systematically varying the Cu loading on TiO_2 [27]. The CH_3OH yield increased with Cu loading, and the highest yield can be achieved by 3 % Cu/TiO_2, which was three times higher than the original TiO_2. Cu can serve as an electron trapper and prohibits the recombination of electron and hole, significantly increasing photoefficiency. However, catalysts with more than 3 wt% Cu loading do not further increase the CH_3OH yield due to its shading effects, consequently reducing the photo-exciting capacity of TiO_2. The activation energy for 3 % Cu/TiO_2 and the original TiO_2 was determined to be 12 and 26 kJ/mol, respectively. The apparent lower activation energy of 3 % Cu/TiO_2 catalyst indicates that the Cu also acts as active species to provide CH_3OH and enhances the photoefficiency of TiO_2 photocatalysts.

In the case of the Pt/TiO_2, the yield of CH_4 increased remarkably when the amount of Pt was increased (0.1–1.0 wt%), but the addition of excess Pt was undesirable for an efficient reaction [13]. Regarding the reaction intermediates, Solymosi et al. have observed the formation of CO_2^- species in bent form under UV irradiation of the Rh/TiO_2 in the presence of CO_2 using FT-IR [28]. The electron transfer from the irradiated catalyst to the adsorbed CO_2 takes place, resulting in the formation of a CO_2^- anion as the key step in the photochemical reduction of CO_2 using metal-loaded TiO_2 semiconductor.

9.5 TiO_2 Single Crystals

With a well-defined catalyst surface such as a single crystal, detailed information on the reaction mechanism can be obtained at the molecular level [2, 15]. Therefore, the photocatalytic reduction of CO_2 with H_2O on rutile-type TiO_2 (100) and TiO_2 (110) single crystal surfaces has been performed [15]. As shown in Table 9.2, the efficiency and selectivity of the photocatalytic reactions strongly depend on the type of TiO_2 single crystal surface. UV irradiation of the TiO_2 (100) single crystal catalyst in the presence of a mixture of CO_2 and H_2O led to the evolution of both CH_4 and CH_3OH at 275 K, whereas only CH_3OH was detected with the TiO_2 (110) single crystal catalyst.

Table 9.2 Yields of the formation of CH_4 and CH_3OH in the photocatalytic reduction of CO_2 (124 μmol g^{-1}) with H_2O (372 μmol g^{-1}) at 275 K

Single crystal of TiO_2	Yield of CH_3OH (μmol/h·g-cat)	Yield of CH_4 (μmol/h·g-cat)
(100)	2.4	3.5
(110)	0.8	0

It is likely that the photogenerated electrons localizing on the surface sites of the excited TiO_2 play a significant role in the photoreduction of CO_2 molecules into intermediate carbon species [2, 15]. The surface Ti atoms may act as a reductive site. According to the surface geometric models for TiO_2 (100) and TiO_2 (110), the atomic ratio (Ti/O) of the top-surface Ti and O atoms, which have geometric spaces large enough to have direct contact with CO_2 and H_2O molecules, is higher on TiO_2 (100) than on TiO_2 (110) surface. In the excited state, the surface with a higher Ti/O surface ratio, i.e., TiO_2 (100), exhibits a more reductive tendency than TiO_2 (110). Such a reductive surface allows a more facile reduction of CO_2 molecules especially for the formation of CH_4. In the HREELS spectrum of a clean TiO_2(100) single crystal surface after UV irradiation in the presence of CO_2 and H_2O, two peaks due to the C–H stretching vibration of the CH_x species and the O–H stretching of the surface hydroxyl groups at around 2,920 and 3,630 cm^{-1}, respectively. On the other hand, only a weak peak assigned to the O–H stretching vibration was observed without UV irradiation, suggesting that UV-light irradiation is indispensable for attaining CO_2 reduction and the formation of the active H and CH_x species.

9.6 Ti-Oxide Anchored on Zeolite (Ion Exchange)

The photocatalyst systems incorporated within the zeolite cavities and frameworks have been proven to be effective for various reactions [29–32]. The Ti-oxide anchored onto zeolite, Ti-oxide/Y-zeolite (1.1 wt% as TiO_2), was prepared by ion exchange with an aqueous titanium ammonium oxalate solution using Y-zeolite ($SiO_2/Al_2O_3 = 5.5$) (ex-Ti-oxide/Y-zeolite) [16–18].

Figure 9.3 shows the Ti K-edge XANES and the Fourier transformation of EXAFS (FT-EXAFS) spectra of the Ti-oxide/Y-zeolites. The XANES spectra of the bulk TiO_2 powder give rise to several well-defined pre-edge peaks attributable to the titanium in a symmetric octahedral environment [33]. The ex-Ti-oxide/Y-zeolite exhibits an intense single pre-edge peak at 4,967 eV, suggesting that the Ti-oxide species exist in a tetrahedral coordination [1–3]. On the other hand, the imp-Ti-oxide/Y-zeolite prepared by the impregnation exhibits three characteristic weak pre-edge peaks attributed to crystalline TiO_2. The FT-EXAFS spectra of the ex-Ti-oxide/Y-zeolite exhibit only peak at around 1.6 Å assigned to the neighboring oxygen atoms (Ti–O) indicating the presence of an isolated Ti-oxide species. These findings indicate that highly dispersed isolated tetrahedral Ti-oxide species are formed on the ex-Ti-oxide/Y-zeolite. On the other hand, the imp-Ti-oxide/Y-zeolite exhibits an intense peak

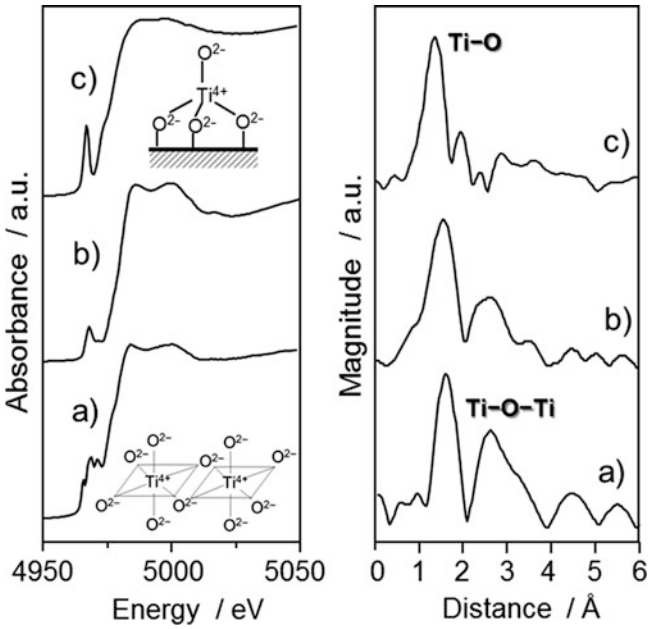

Fig. 9.3 Ti K-edge XANES and FT-EXAFS spectra of anatase TiO_2 powder (*a*), imp-Ti-oxide/Y-zeolite (10.0 wt% as TiO_2) (*b*), and the ex-Ti-oxide/Y-zeolite (*c*)

assigned to the neighboring titanium atoms (Ti–O–Ti) suggestive of the aggregation of the Ti-oxide species.

The photoluminescence spectra of the ex-Ti-oxide/Y-zeolite at 77 K are shown in Fig. 9.4. Excitation by light at around 250–280 nm brought about an electron transfer from the oxygen to titanium ion, resulting in the formation of pairs of the trapped hole center (O^-) and an electron center (Ti^{3+}) [1–3]. The observed photoluminescence is attributed to the radiative decay process from the charge-transfer excited state of the Ti-oxide moieties in a tetrahedral coordination geometry, $(Ti^{3+}—O^-)^*$, to their ground state [34, 35]. The addition of H_2O or CO_2 molecules onto the anchored Ti-oxide species leads to the efficient quenching of the photoluminescence. Such an efficient quenching suggests not only that tetrahedrally coordinated Ti-oxide species locate at positions accessible to the added CO_2 or H_2O but also that CO_2 or H_2O interacts and/or reacts with the Ti-oxide species in both its ground and excited states. Because the addition of CO_2 led to a less effective quenching than that with the addition of H_2O, the interaction of the emitting sites with CO_2 was weaker than that with H_2O.

UV irradiation of powdered TiO_2 and Ti-oxide/Y-zeolite catalysts in the presence of a mixture of CO_2 and H_2O led to the evolution of CH_4 and CH_3OH at 328 K, as well as trace amounts of CO, C_2H_4, and C_2H_6 [16–18]. The specific photocatalytic activities for the formation of CH_4 and CH_3OH are shown in Fig. 9.5. The ex-Ti-oxide/Y-zeolite exhibits a high activity and a high selectivity for the formation of CH_3OH, while the formation of CH_4 was predominated on bulk TiO_2 as well as on

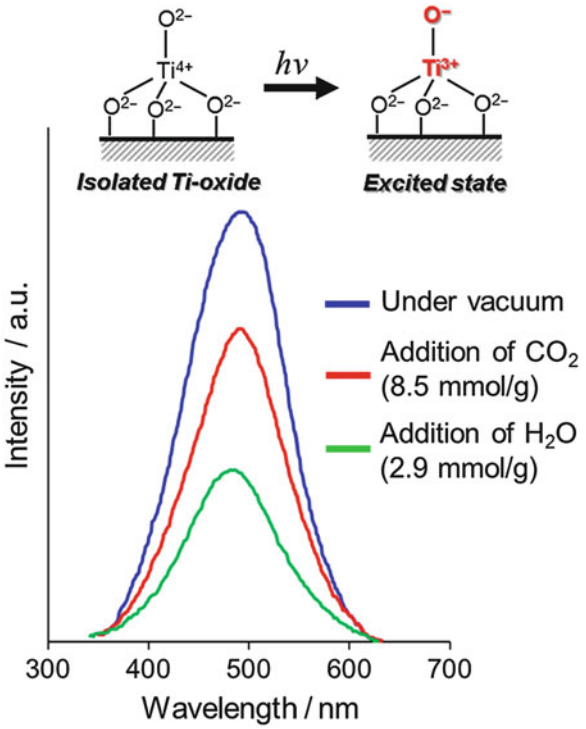

Fig. 9.4 Photoluminescence spectrum of the ex-Ti-oxide/Y-zeolite catalyst (a) and the effects of the addition of CO_2 and H_2O. Measured at 77 K, excitation at 290 nm, and emission monitored at 490 nm

the imp-Ti-oxide/Y-zeolite. The deposition of Pt improved the photocatalytic activity, but the CH_3OH selectivity significantly decreased. These findings clearly suggest that the tetrahedrally coordinated Ti-oxide species act as active photocatalysts for the reduction of CO_2 with H_2O exhibiting a high selectivity toward CH_3OH.

UV irradiation of the anchored Ti-oxide catalyst in the presence of CO_2 and H_2O at 77 K led to the appearance of ESR signals due to the Ti^{3+} ions, H atoms, and carbon radicals [2, 3]. After the disappearance of these ESR signals in this system at around 275 K, the formation of CH_4 and CH_3OH was observed. From these results, the reaction mechanism in the photocatalytic reduction of CO_2 with H_2O on the highly dispersed Ti-oxide catalyst can be proposed as shown in Scheme 9.1: CO_2 and H_2O molecules interact with the excited state of the photoinduced $(Ti^{3+}—O^{-})^*$ species and the reduction of CO_2 and the decomposition of H_2O proceed competitively. Furthermore, H atoms and OH• radicals are formed from H_2O and such radicals react with the carbon species formed from CO_2 to produce CH_4 and CH_3OH.

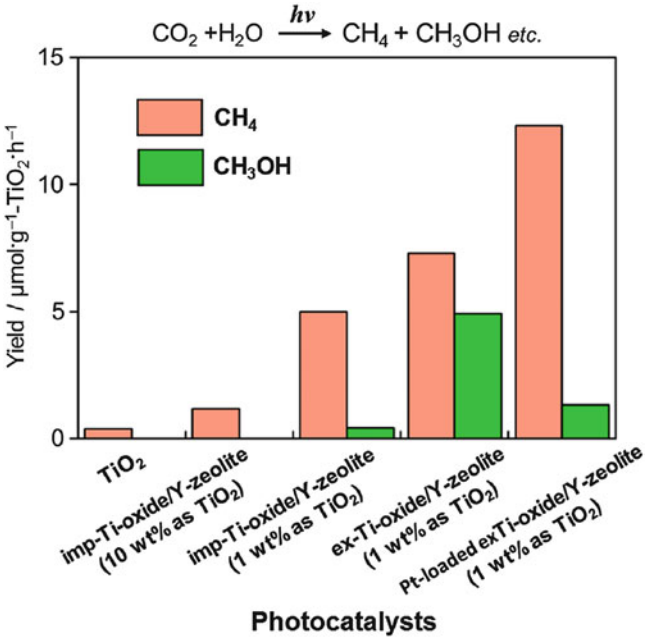

Fig. 9.5 The product distribution of the photocatalytic reduction of CO_2 with H_2O on anatase TiO_2 powder, the imp-Ti-oxide/Y-zeolite (10 wt% as TiO_2), the imp-Ti-oxide/Y-zeolite (1 wt% as TiO_2), the ex-Ti-oxide/Y-zeolite (1 wt% as TiO_2), and the Pt-loaded ex-Ti-oxide/Y-zeolite catalysts

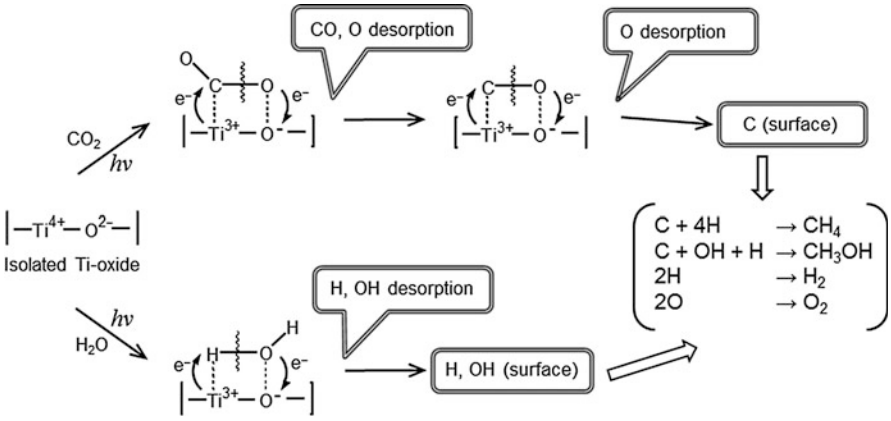

Scheme 9.1 Schematic illustration of the photocatalytic reduction of CO_2 with H_2O on the anchored titanium oxide species

9.7 Ti-Containing Zeolite and Mesoporous Molecular Sieves

The Ti-oxide species prepared within the ordered silica frameworks have revealed a unique local structure as well as a high selectivity in the oxidation of organic substances with hydrogen peroxide [34–36]. Hydrothermally synthesized Ti-containing zeolites (TS-1, Ti-Beta) and mesoporous molecular sieves (Ti-MCM, Ti-HMS, Ti-FSM) have been subjected to the photocatalytic reduction CO_2 with H_2O [18–22, 36–38].

In situ photoluminescence, ESR, UV–VIS and XAFS investigations indicated that the Ti-oxide species in the Ti-mesoporous molecular sieves (Ti-MCM-41 and Ti-MCM-48) and in the TS-1 zeolite are highly dispersed within the zeolite framework and exist in a tetrahedral coordination. Upon excitation with UV light at around 250–280 nm, these catalysts exhibit photoluminescence spectra at around 480 nm. The addition of CO_2 or H_2O onto these catalysts results in a significant quenching of the photoluminescence, suggesting the excellent accessibility of the CO_2 and H_2O to the Ti-oxide species [18–21].

UV irradiation of the Ti-mesoporous molecular sieves and the TS-1 zeolite in the presence of CO_2 and H_2O also led to the formation of CH_3OH and CH_4 as the main products [18–21]. The yields of CH_3OH and CH_4 per unit weight of the Ti-based catalysts are shown in Fig. 9.6. It can be seen that Ti-MCM-48 exhibits much higher activity than either TS-1 or Ti-MCM-41. The higher activity and selectivity for the formation of CH_3OH attained with the Ti-MCM-48 than that with the other catalysts may be due to the combined contribution of the high dispersion state of the Ti-oxide species and the large pore size with a three-dimensional channel structure: TS-1 has a smaller pore size (ca. 5.7 Å) and a three-dimensional channel structure; Ti-MCM-41 has a large pore size (>20 Å) but one-dimensional channel structure; and Ti-MCM-48 has both a large pore size (>20 Å) and three-dimensional channels. These results strongly suggest that mesoporous molecular sieves containing highly dispersed Ti-oxide species are promising candidates as effective photocatalysts.

The effect of Pt loading on the photocatalytic activity of Ti-containing mesoporous silica has also been investigated, and the changes in the yields of CH_4 and CH_3OH formation are shown in Fig. 9.6. The deposition of Pt onto the Ti-containing zeolites is effective for promoting the photocatalytic activity, but the formation of only CH_4 is promoted [18].

Ti-containing zeolite, Ti-Beta, has attracted much attention because of their large-pore structure compared to the Y-zeolite [36–38]. The other characteristic feature is that the H_2O affinity of Ti-Beta zeolites can be changed significantly depending on the preparation methods, and their hydrophobic–hydrophilic properties can modify the catalytic performances [36–38]. As shown in Fig. 9.7, the photocatalytic reduction of CO_2 with H_2O was found to proceed in the gas phase at 323 K with different activity and selectivity on hydrophilic Ti-Beta(OH) and hydrophobic Ti-Beta(F) zeolites prepared in the OH^- and F^- media, respectively.

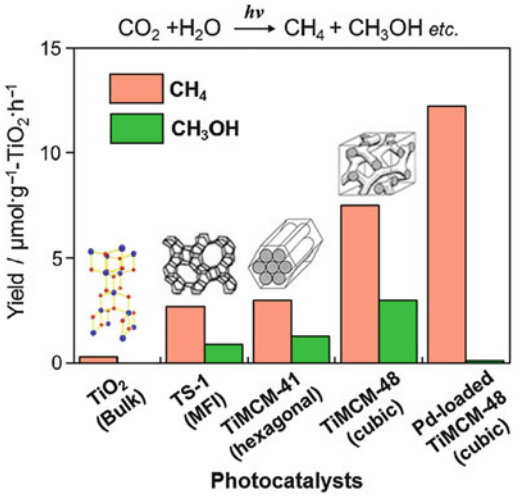

Fig. 9.6 The product distribution of the photocatalytic reduction of CO_2 with H_2O on TiO_2 powder, TS-1, Ti-MCM-41, Ti-MCM-48, and the Pt-loaded Ti-MCM-48 catalysts

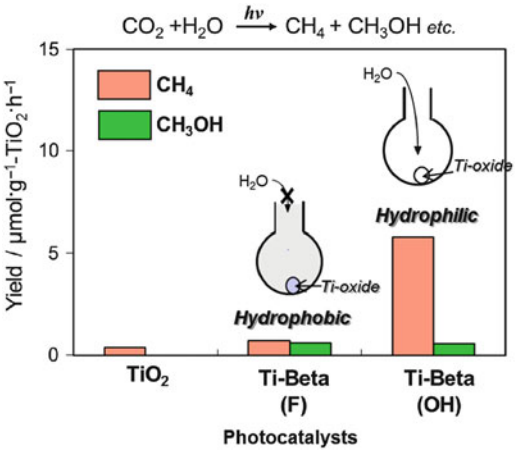

Fig. 9.7 The product distribution of the photocatalytic reduction of CO_2 with H_2O on Ti-Beta(F), Ti-Beta(OH), and TiO_2 powder (P-25) as the reference catalyst

The higher activity for the formation of CH_4 observed with Ti-Beta(OH) and the higher selectivity for the formation of CH_3OH observed with the Ti-Beta(F) may be attributed to the different abilities of zeolite pores on the H_2O affinity. These results suggest that the affinity of the H_2O molecules to adsorb on the zeolite is one of important factors for the selectivity in the photocatalytic reduction of CO_2 and H_2O.

For the reduction of CO_2 with H_2O on the Ti-containing zeolite and mesoporous molecular sieves, a similar reaction pathway with Ti-oxide anchored on zeolite is proposed by considering ESR spectroscopy at 77 K, in which CO_2 reduction and

H_2O splitting proceed competitively at the LMCT-excited Ti—O centers: CO_2 is reduced to CO and subsequently to C radicals, while H_2O photodecomposes to H and OH radicals. Reaction of H and OH radicals with carbon species is thought to yield CH_3OH and CH_4. Frei and co-workers carried out further mechanistic investigations by monitoring the visible light-induced reaction of $^{13}CO_2$ and H_2O gas mixtures in the framework Ti-MCM-41 molecular sieve with in situ FT-IR spectroscopy at room temperature [39]. ^{12}CO gas along with ^{13}CO were observed as the products by infrared, and the growth of ^{13}CO depended linearly on the photolysis laser power. This points out the presence of small amounts of carbonaceous residues on the high-surface area mesoporous silicates. H_2O was also confirmed as the stoichiometric electron donor. These results suggest that CO is a single-photon, 2-electron-transfer product of CO_2 at framework Ti centers with H_2O acting as a direct electron donor. By considering this, the mechanism is proposed as follows: Excitation of the framework Ti^{4+} centers leads to photoinduced $(Ti^{3+}—O^-)^*$ species. Electron transfer from transient Ti^{3+} to CO_2 splits the molecule into CO and O^-. The latter is spontaneously protonated by a Si–OH group or H^+ cogenerated upon H_2O oxidation to yield a surface OH radical. Another surface OH radical is formed as a result of the simultaneous H_2O oxidation by the framework oxygen hole. The OH radicals either combine to yield H_2O_2 or dismutate to give O_2 and H_2O.

9.8 Ti-Oxide Anchored on Porous Silica Glass (CVD)

The Ti-oxide anchored onto porous silica glass (PVG) plate was prepared using a facile reaction of $TiCl_4$ with the surface OH groups on the transparent porous Vycor glass (Corning Code 7930) in the gas phase at 453–473 K, followed by treatment with H_2O vapor to hydrolyze the anchored compound [11–13]. UV irradiation of the anchored Ti-oxide catalysts in the presence of a mixture of CO_2 and H_2O led to the evolution of CH_4, CH_3OH, and CO at 323 K. The total yield was larger under UV irradiation at 323 K than at 275 K. The efficiency of the photocatalytic reaction strongly depends on the ratio of H_2O/CO_2, and its activity increases with increasing the H_2O/CO_2 ratio; however, an excess amount of H_2O suppresses the reaction rates. Figure 9.8 shows the effect of the number of anchored Ti–O layers on the absorption edge in the UV–VIS spectra of the catalysts and the efficiency of the photocatalytic reactions as well as the relative yields of the photoluminescence. It was proven that only catalysts with highly dispersed monolayer Ti-oxide exhibit high photocatalytic activity and photoluminescence at around 480 nm. Only the tetrahedrally coordinated Ti-oxide species exhibit photoluminescence emission upon excitation at around 250–280 nm. These findings also clearly suggest that the tetrahedrally coordinated Ti-oxide species function as active photocatalysts for the reduction of CO_2 with H_2O.

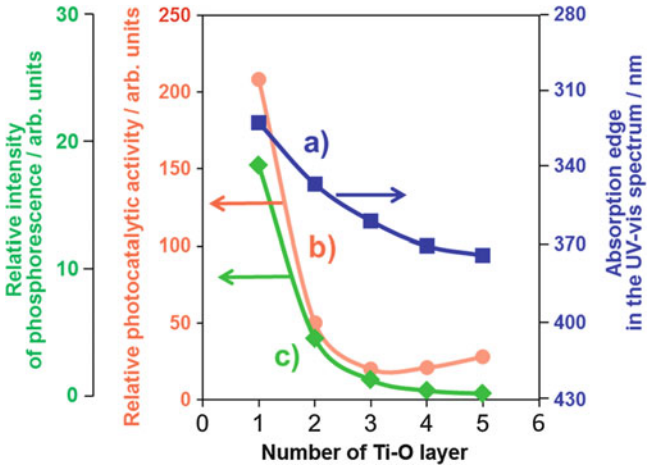

Fig. 9.8 The effects of the number of the Ti–O layers of the anchored titanium oxide catalysts on the absorption edge of the catalysts (*a*), the reaction yields (*b*), and the relative yields of the photoluminescence (*c*)

9.9 Ti-Containing Porous Silica Thin Film

In the syntheses of zeolites and mesoporous molecular sieves, the morphology of these materials was mainly in powdered form. However, powdered material systems are difficult to handle for practical use as photocatalysts. Therefore, the synthesis of transparent porous silica thin films is a subject of current interest. Such transparent porous silica thin films have a larger surface area, in contrast to metal oxide thin films on a quartz substrate, and can realize the efficient absorption of light, showing that they have potential for use as effective photocatalysts.

Self-standing Ti-containing porous silica (PS) thin films with different pore structures and Ti contents were synthesized by a solvent evaporation method. Ti-PS(h, 25) and Ti-PS(c, 50) mean hexagonal and cubic structure with a Si/Ti ratio of 25 and 50, respectively [40, 41]. The synthesized thin films are colorless and completely transparent. Mesoporous structure was confirmed by a characteristic diffraction peak at around 2–3° associated with the d_{100} spacing.

UV irradiation of these Ti-containing porous silica thin films in the presence of CO_2 and H_2O at 323 K led to the formation of CH_4 and CH_3OH as well as CO and O_2 as minor products. Ti-PS(h, 50) thin film was proven to be the most effective photocatalyst with a high quantum yield of 0.28 %, which was larger than the Ti-MCM-41 powder catalyst even with the same pore structure (Fig. 9.9). This quantum yields obtained with transparent Ti-PS (50) thin film photocatalyst has been improved in contrast to the value obtained with the titanium oxide anchored on transparent porous silica glass (0.02 %). In powdered form, the effect of the scattering of light on the particle surface would be large so that effective light

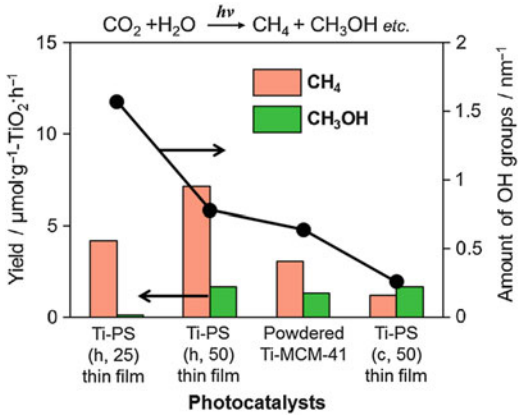

Fig. 9.9 The product distribution of the photocatalytic reduction of CO_2 with H_2O and amount of surface OH groups on Ti-PS(h, 25), Ti-PS(h, 50), powdered Ti-MCM-41, and Ti-PS(c, 50)

absorption and measurement may not be realized. Thus, the high photocatalytic activity of such thin films can be attributed to the efficient absorption of UV light due to its high transparency. From FT-IR investigations, it was found that these Ti-containing porous silica thin films had different concentrations of surface OH groups and showed different adsorption properties for the H_2O molecules toward the catalyst surface: photocatalysts having small amounts of surface OH groups showed high selectivity for the formation of CH_3OH.

9.10 Ti/Si Binary Oxide (Sol–Gel)

Ti/Si binary oxides involving different Ti contents were prepared by the sol–gel method using mixtures of tetraethylorthosilicate and titanium *iso*propoxide. Ti/Si binary oxides with only a small Ti contents exhibited the photoluminescence emission at around 480 nm upon excitation at around 280 nm [22, 42]. UV irradiation of the Ti/Si binary oxide catalysts in the presence of a gaseous mixture of CO_2 and H_2O led to the formation of CH_4 and CH_3OH as the main products. A parallel relationship between the specific photocatalytic activities of the titanium oxide species and the photoluminescence yields of the Ti/Si binary oxides was observed. This phenomenon clearly indicates that the appearance of high photocatalytic activity for the binary oxides is closely associated with the formation of the charge-transfer excited complex due to the highly dispersed tetrahedral Ti-oxide species.

The XAFS, ESR, and photoluminescence investigations of the Ti/Si binary oxide indicated that these catalysts prepared by the sol–gel method can keep tetrahedral coordination geometry of Ti-oxide species until the TiO_2 content approaches up to approximately 20 wt%. Consequently, the Ti/Si binary oxides having a high Ti content can be successfully utilized as active photocatalysts for the efficient reduction of CO_2 with H_2O in the gas–solid system.

9.11 Visible Light-Sensitive TiO_2-Based Catalysts

The development of visible light-sensitive photocatalysts was intensively pursued since the pure TiO_2 and Ti-oxide species only shows fascinating photocatalytic activities under UV-light irradiation, which limit the utilization of a small UV fraction of natural solar light. One of the most promising strategies to use higher wavelength of the solar spectrum is the dye sensitization of TiO_2. The organometallic dye, especially (2,2′-bipyridine) ruthenium (II) chloride hexahydrate, attached TiO_2 absorb sunlight and injects electrons into the conduction band of TiO_2, which ultimately promote the CO_2 reduction to produce CH_4 [43]. It was also reported that the perylene diimide derivatives have shown high light-harvesting capacity similar to the Ru complex dye.

Nguyen et al. found substantial improvements in the photoactivity of metal-doped TiO_2–SiO_2 mixed oxide-based photocatalysts toward CO_2 photoreduction in the presence of H_2O and concentrated sunlight in an optical fiber photoreactor (OFPR) [44]. Fe atoms are introduced into the TiO_2–SiO_2 lattice during sol–gel process, resulting in the full visible light absorption as well as the effect on product selectivity of the obtained catalyst. Cu–Fe/TiO_2 catalyst mainly produced ethylene with the quantum yield of 0.024 %, whereas Cu–Fe/TiO_2–SiO_2 catalyst exhibited favorable methane production with the quantum yield of 0.05 %. The overall energy efficiency is found to be higher on Cu–Fe/TiO_2–SiO_2 (0.018 %) than on its Cu–Fe/TiO_2 (0.016 %). The superior photoactivity of Cu–Fe/TiO_2–SiO_2 catalyst under natural sunlight could be ascribed to the efficient charge-transfer mechanism between TiO_2 and Cu as well as Fe as co-dopants and its full absorption of visible light.

9.12 Various Metal Oxide Photocatalysts

The reviews concerning the photocatalytic reduction of CO_2 using various metallic oxides other than TiO_2 have been previously summarized by Navalon et al. [45] In general, ZnO and NiO are widely known as versatile oxide semiconductors except for TiO_2. Because these ZnO and NiO semiconductors possess negatively high conduction band potential compared to the TiO_2 (TiO_2, −0.29 V; ZnO, −0.31 V; NiO, −0.50 V at pH 7) [46]. Yahaya et al. focused on these conduction band potential for efficient CO_2 reduction, and the photocatalytic reduction of CO_2 to CH_3OH was performed in an aqueous suspension of these oxide semiconductors under laser light irradiation at 355 nm [47]. The ZnO and NiO semiconductors exhibited more efficient CH_3OH production performance than the TiO_2. The amounts of produced CH_3OH decreased with irradiation time when TiO_2 and ZnO were used as photocatalysts, indicating that the produced CH_3OH was further oxidized to HCHO, HCOOH, or CO_2 by the high oxidation ability of these materials, while no decrease of produced CH_3OH was confirmed in the presence of the NiO semiconductor. In addition, they discovered that more efficient CH_3OH

production was achieved to convert CO_2 into H_2CO_3, because the pH of the system decreases by production of H_2CO_3 (dissolution of CO_2), resulting in the shift of conduction band edge to more positive value.

Novel oxide photocatalysts by composite compounds of various metal species were also reported for photoreduction of CO_2 [48]. Various cocatalyst nanoparticles such as NiO_x, Ru, Cu, Au, or Ag were loaded on $ALa_4Ti_4O_{15}$ (A = Ca, Sr, or Ba). Among those synthesized, 2 wt% Ag loaded on $BaLa_4Ti_4O_{15}$ ($Ag/BaLa_4Ti_4O_{15}$) exhibited the highest CO_2 reduction performance, resulting in the formation of CO as a main product. The Ag cocatalyst acted as a reduction site to produce CO from CO_2. Interestingly, the photocatalytic activity for CO_2 reduction strongly depends on the loading method of Ag nanoparticles. The small-size Ag nanoparticles (10 nm) were prepared on the edge of plate particle of the $BaLa_4Ti_4O_{15}$ by liquid-phase chemical reduction method, and the performance of photocatalytic CO_2 reduction was significantly improved compare to the $Ag/BaLa_4Ti_4O_{15}$ using conventional method such as impregnation or photodeposition. It is concluded that the separation of reaction sites (reduction and oxidation) and the loading of small-size Ag cocatalyst on the edge of plate play important roles to achieve efficient activation of CO_2 reduction using $Ag/BaLa_4Ti_4O_{15}$ photocatalyst.

As discussed in Sect. 9.11, the development of visible light-sensitive photocatalyst is also absolutely imperative for more efficient CO_2 reduction. The unique photocatalyst system for CO_2 reduction using composite oxide of $Pt/ZnAl_2O_4$ modified with mesoporous ZnGaNO was reported by Yan et al. [49]. The photocatalytic reduction of CO_2 to CH_4 was efficiently confirmed in the presence of H_2O under visible light irradiation ($\lambda > 420$ nm), because this novel and unique photocatalyst possesses high CO_2 adsorption property derived from mesoporous structure, basicity, and visible light absorption ability by narrow band gap structure to achieve efficient CO_2 reduction. This photocatalytic activity is about seven times higher than that of Pt-loaded N-doped TiO_2 known as versatile visible light-sensitive photocatalyst.

9.13 Localized Surface Plasmon Resonance-Enhanced Photocatalyst

Au nanoparticle can absorb visible and infrared light in particular regions due to localized surface plasmon resonance (LSPR) [50, 51]. In simple terms, LSPR is made up of collective oscillations of free electrons in metal NPs driven by the electromagnetic field of incident light [4]. This unique characteristic has given rise to a new approach to the fabrication of visible light-sensitive photocatalysts, known as plasmonic photocatalysts, through the deposition of Au nanoparticle onto suitable semiconductors [52]. It has been proposed that in the case of Au/TiO_2, at an excitation wavelength corresponding to the LSPR of Au, the Au nanoparticle absorb photons and inject photogenerated electrons into the TiO_2 conduction band [53].

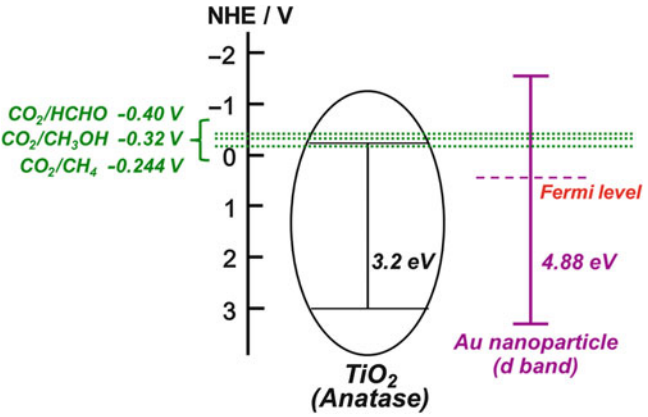

Fig. 9.10 The energy level of anatase-type TiO_2 and Au nanoparticle and reduction of CO_2 to HCHO, CH_3OH, or CH_4

The photocatalytic reduction of CO_2 to CH_4 using the unique LSPR property of Au/TiO_2 was recently performed by Hou et al. [54, 55]. In this system, the main product was CH_4, but the methanol and formaldehyde were also observed. When the light ($\lambda = 532$ nm) matched to the LSPR absorption of Au nanoparticle was utilized in this system, the reduction efficiency of CO_2 was about 24 times higher than that of bare TiO_2. They discussed that the excited electrons produced in the Au nanoparticles by the LSPR did not directly transfer to the conduction band of TiO_2. However, when the photon possessing high enough energy to excite the electrons in d-band of Au nanoparticles was irradiated, the charge was directly transferred between Au nanoparticle and TiO_2 (Fig. 9.10). Since the LSPR can absorb light of long-wavelength region, this unique photocatalytic system is one of promising approach for efficient CO_2 reduction by beneficial use of photo-energy.

9.14 Conclusions

In this chapter, we have focused on the progress in the very stimulating field of the photocatalytic reduction of CO_2 with H_2O on various types of Ti-oxide catalysts. Upon UV-light irradiation, the reactions on TiO_2 powders in the presence of gaseous CO_2 and H_2O at 275 K produced CH_4 as the major product, while on the highly dispersed titanium oxide anchored on porous glass or ordered porous silicas, the formations of CH_3OH as well as CH_4 were observed as the major products. In situ spectroscopic studies of the system indicated that the photocatalytic reduction of CO_2 with H_2O is linked to a much higher activity of the charge-transfer excited state, i.e., $(Ti^{3+}—O^{-})^*$ of the tetrahedral coordinated Ti-oxide species formed on the surface. Owing to the dramatically growing nature of this research field, we expect that the

design strategy described here can offer a helpful overview to the readers in this fascinating area. In recent report, the highly efficient reduction of CO_2 was achieved using various oxide semiconductors or the LSPR property of metallic nanoparticles. These photocatalytic systems are expected for solution of various global environment problems including CO_2 problem.

References

1. Anpo M, Yamashita H (1996) Photochemistry of surface species anchored on solid surface. In: Anpo M (ed) Surface photochemistry. Wiley, Chichester, pp 117–164
2. Schiavello M (ed) (1997) Heterogeneous photocatalysts. Wiley, Chichester
3. Anpo M (2000) Photofunctional zeolites. NOVA, New York
4. Anpo M, Yamashita H, Zhang SG (1996) Photoinduced surface chemistry. Curr Opin Solid State Mater Sci 1:630–635
5. Anpo M (1989) Photocatalysis on small particle TiO_2 catalysts. Reaction intermediates and reaction mechanisms. Res Chem Intermed 11:67–106
6. Anpo M, Ichihashi Y, Takeuchi M, Yamashita H (1998) Design of unique titanium oxide photocatalysts by an advanced metal ion-implantation method and photocatalytic reactions under visible light irradiation. Res Chem Intermed 24:143–149
7. Yamashita H, Ichihashi Y, Takeuchi M, Kishiguchi S, Anpo M (1999) Characterization of metal ion-implanted titanium oxide photocatalysts operating under visible light irradiation. J Synchrotron Radiat 6:451–452
8. Yamashita H, Honda M, Harada M, Ichihashi Y, Anpo M (1998) Preparation of titanium oxide photocatalysts anchored on porous silica glass by a metal ion-implantation method and their photocatalytic reactivities for the degradation of 2-propanol diluted in water. J Phys Chem B 102:10707–10711
9. Inoue T, Fujishima A, Konishi S, Honda K (1979) Photoelectrocatalytic reduction of carbon dioxide in aqueous suspensions of semiconductor powders. Nature 277:637–640
10. Halmann M (1983) Photochemical fixation of carbon dioxide. In: Grätzel M (ed) Energy resources through photochemistry and catalysis. Academic, New York, pp 507–565
11. Anpo M, Chiba K (1992) Photocatalytic reduction of carbon dioxide on anchored titanium oxide catalysts. J Mol Catal 74:207–302
12. Yamashita H, Shiga A, Kawasaki S, Ichihashi Y, Ehara S, Anpo M (1995) Photocatalytic synthesis of CH_4 and CH_3OH from CO_2 and H_2O on highly dispersed active titanium oxide catalysts. Energy Conv Manag 36:617–620
13. Anpo M, Yamashita H, Ichihashi Y, Ehara S (1995) Photocatalytic reduction of CO_2 with H_2O on various titanium oxide catalysts. J Electroanal Chem 396:21–26
14. Yamashita H, Nishiguchi H, Kamada N, Anpo M, Teraoka Y, Hatano H, Ehara S, Kikui K, Palmisano L, Sclafani A, Schiavello M, Fox MA (1994) Photocatalytic reduction of CO_2 with H_2O on TiO_2 and Cu/TiO_2 catalysts. Res Chem Intermed 20:815–823
15. Yamashita H, Kamada N, He H, Tanaka K, Ehara S, Anpo M (1994) Reduction of CO_2 with H_2O on $TiO_2(100)$ and $TiO_2(110)$ single crystals under UV-irradiation. Chem Lett 1994 (5):855–858
16. Anpo M, Yamashita H, Ichihashi Y, Fujii Y, Honda M (1997) Photocatalytic reduction of CO_2 with H_2O on titanium oxides anchored within micropores of zeolites: effects of the structure of the active sites and the addition of Pt. J Phys Chem B 101:2632–2636
17. Anpo M, Yamashita H, Fujii Y, Ichihashi Y, Zhang SG, Park DR, Ehara S, Park SE, Chang JS, Yoo JW (1998) Photocatalytic reduction of CO_2 with H_2O on titanium oxides anchored within zeolites. Stud Surf Sci Catal 114:177–182

18. Yamashita H, Fuji Y, Ichihashi Y, Zhang SG, Ikeue K, Park DR, Koyano K, Tatsumi T, Anpo M (1998) Selective formation of CH_3OH in the photocatalytic reduction of CO_2 with H_2O on titanium oxides highly dispersed within zeolites and mesoporous molecular sieves. Catal Today 45:221–227
19. Anpo M, Zhang SG, Fujii Y, Ichihashi Y, Yamashita H, Koyano K, Tatsumi T (1998) Photocatalytic reduction of CO_2 with H_2O on Ti-MCM-41 and Ti-MCM-48 mesoporous zeolite catalysts. Catal Today 44:327–332
20. Ikeue K, Yamashita H, Anpo M (1999) Photocatalytic reduction of CO_2 with H_2O on titanium oxides prepared within the FSM-16 mesoporous zeolite. Chem Lett 1999(11):1135–1136
21. Yamashita H, Ikeue K, Takewaki T, Anpo M (2002) In situ XAFS studies on the effects of the hydrophobic-hydrophilic properties of Ti-beta zeolites in the photocatalytic reduction of CO_2 with H_2O. Top Catal 18:95–100
22. Yamashita H, Kawasaki S, Fujii Y, Ichihashi Y, Ehara S, Park SE, Chang JS, Yoo JW, Anpo M (1998) Photocatalytic reduction of CO_2 with H_2O on Ti/Si binary oxide catalysts prepared by the sol-gel method. Stud Surf Sci Catal 114:561–564
23. Saladin F, Forss L, Kamber I (1995) Photosynthesis of CH_4 at a TiO_2 surface from gaseous H_2O and CO_2. J Chem Soc Chem Commun 5:533–534
24. Anpo M, Tomonari M, Fox MA (1989) In situ photoluminescence of titania as a probe of photocatalytic reactions. J Phys Chem 93:7300–7303
25. Yamashita H, Ichihashi Y, Harada M, Stewart G, Fox MA, Anpo M (1996) Photocatalytic degradation of 1-octanol on anchored titanium oxide and on TiO_2 powder catalysts. J Catal 158:97–101
26. Frese KW (1991) Electrochemical reduction of carbon dioxide at intentionally oxidized copper electrodes. J Electrochem Soc 138:3338–3343
27. Slamet HW, Nasution E, Purnama E, Kosela S, Gunlazuardi J (2005) Photocatalytic reduction of CO2 on copper-doped titania catalysts prepared by improved-impregnation method. Catal Commun 6:313–319
28. Raskö J, Solymosi F (1994) Infrared spectroscopic study of the photoinduced activation of CO_2 on TiO_2 and Rh/TiO_2 catalysts. J Phys Chem 98:7147–7152
29. Anpo M, Matsuoka M, Shioya Y, Yamashita H, Giamello E, Morterra C, Che M, Patterson HH, Webber S, Ouellette S, Fox MA (1994) Preparation and characterization of the Cu^+/ZSM-5 catalyst and its reaction with NO under UV irradiation at 275 K. In situ photoluminescence, EPR, and FT-IR investigations. J Phys Chem 98:5744–5750
30. Yamashita H, Matsuoka M, Tsuji K, Shioya Y, Anpo M, Che M (1996) In-situ XAFS, photoluminescence, and IR investigations of copper ions included within various kinds of zeolites. Structure of Cu(I) ions and their interaction with CO molecules. J Phys Chem 100:397–402
31. Yamashita H, Ichihashi Y, Anpo M, Hashimoto M, Louis C, Che M (1996) Cavities: the structure and role of the active sites. J Phys Chem 100:16041–16044
32. Yamashita H, Zhang SG, Ichihashi Y, Matsumura Y, Souma S, Tatsumi T, Anpo M (1997) Photocatalytic decomposition of NO at 275 K on titanium oxide catalysts anchored within zeolite cavities and framework. Appl Surf Sci 121:305–309
33. Farges F, Brown GE Jr, Rehr JJ (1996) Coordination chemistry of Ti(IV) in silicate glasses and melts: I. XAFS study of titanium coordination in oxide model compounds. Geochim Cosmochim Acta 60:3023–3060
34. Anpo M, Aikawa N, Kubokawa Y, Che M, Louis C, Giamello E (1985) Photoluminescence and photocatalytic activity of highly dispersed titanium oxide anchored onto porous Vycor glass. J Phys Chem 89:5017–5021
35. Anpo M, Aikawa N, Kubokawa Y, Che M, Louis C, Giamello E (1985) Photoformation and structure of oxygen anion radicals (O_2^-) and nitrogen-containing anion radicals adsorbed on highly dispersed titanium oxide anchored onto porous Vycor glass. J Phys Chem 89:5689–5694
36. Takewaki T, Hwang SJ, Yamashita H, Davis ME (1999) Synthesis of BEA-type molecular sieves using mesoporous materials as reagents. Micropor Mesopor Mater 32:265–273

37. Camblor MA, Corma A, Esteve P, Martines M, Valencia S (1997) Epoxidation of unsaturated fatty esters over large-pore Ti-containing molecular sieves as catalysts: important role of the hydrophobic-hydrophilic properties of the molecular sieve. Chem Commun 33:795–796
38. Tatsumi T, Jappar N (1998) Properties of Ti-beta zeolites synthesized by dry-gel conversion and hydrothermal methods. J Phys Chem B 102:7126–7131
39. Lin W, Han H, Frei H (2004) CO_2 splitting by H_2O to CO and O_2 under UV light in TiMCM-41 silicate sieve. J Phys Chem B 108:18269–18273
40. Ikeue K, Nozaki S, Ogawa M, Anpo M (2002) Photocatalytic reduction of CO_2 with H_2O on Ti-containing porous silica thin film photocatalysts. Catal Lett 80:111–114
41. Ikeue K, Nozaki S, Ogawa M, Anpo M (2002) Characterization of self-standing Ti-containing porous silica thin films and their reactivity for the photocatalytic reduction of CO_2 with H_2O. Catal Today 74:241–248
42. Yamashita H, Kawasaki S, Ichihashi Y, Harada M, Anpo M, Stewart G, Fox MA, Louis C, Che M (1998) Characterization of titanium-silicon binary oxide catalysts prepared by the sol-gel method and their photocatalytic reactivity for the liquid-phase oxidation of 1-octanol. J Phys Chem B 102:5870–5875
43. Ozcan O, Yukruk F, Akkaya EU, Uner D (2007) Dye sensitized CO2 reduction over pure and platinized TiO2. Top Catal 44:523–528
44. Nguyen TH, Wu JCS (2008) Photoreduction of CO2 to fuels under sunlight using optical-fiber reactor. Sol Energy Mater Sol Cells 92:864–872
45. Navalon S, Dhakshinamoorthy A, Alvaro M, Garcia H (2013) You have free access to this content photocatalytic CO_2 reduction using non-titanium metal oxides and sulfides. Chem Sus Chem 6:562–577
46. Xu Y, Schoonen MAA (2000) The absolute energy positions of conduction and valence bands of selected semiconducting minerals. Am Mineral 85:543–556
47. Yahaya AH, Gondal MA, Hameed A (2004) Selective laser enhanced photocatalytic conversion of CO2 into methanol. Chem Phys Lett 400:206–212
48. Iizuka K, Wato T, Miseki Y, Saito K, Kudo A (2011) Photocatalytic reduction of carbon dioxide over Ag cocatalyst-loaded $ALa_4Ti_4O1_5$ (A = Ca, Sr, and Ba) using water as a reducing reagent. J Am Chem Soc 133:20863–20868
49. Yan S, Yu H, Wang N, Li Z, Zou Z (2012) Efficient conversion of CO_2 and H_2O into hydrocarbon fuel over $ZnAl_2O_4$-modified mesoporous ZnGaNO under visible light irradiation. Chem Commun 48:1048–1050
50. Mori K, Kawashima M, Che M, Yamashita H (2010) Enhancement of the photoinduced oxidation activity of a ruthenium(II) complex anchored on silica-coated silver nanoparticles by localized surface plasmon resonance. Angew Chem Int Ed 49:8598–8601
51. Fuku K, Hayashi R, Takakura S, Kamegawa T, Mori K, Yamashita H (2013) The synthesis of size- and color-controlled silver nanoparticles by using microwave heating and their enhanced catalytic activity by localized surface plasmon resonance. Angew Chem Int Ed 52:7446–7450
52. Cushing SK, Li JT, Meng FK, Senty TR, Suri S, Zhi MJ, Li M, Bristow AD, Wu NQ (2012) Photocatalytic activity enhanced by plasmonic resonant energy transfer from metal to semiconductor. J Am Chem Soc 134:15033–15041
53. Tanaka A, Sakaguchi S, Hashimoto K, Kominami H (2012) Preparation of Au/TiO_2 exhibiting strong surface plasmon resonance effective for photoinduced hydrogen formation from organic and inorganic compounds under irradiation of visible light. Catal Sci Technol 2:907–909
54. Hou WB, Hung WH, Pavaskar P, Goeppert A, Aykol M, Cronin SB (2011) Photocatalytic conversion of CO_2 to hydrocarbon fuels via plasmon-enhanced absorption and metallic interband transitions. ACS Catal 1:929–936
55. Hou WB, Cronin SB (2013) A review of surface plasmon resonance-enhanced photocatalysis. Adv Funct Mater 23:1612–1619